REPORT

AD-A279 348

Form Approved
OMB No. 0704-0188

1. AGENCY USE ONLY (Leave blank)	2. REPORT DATE	3. REPORT TYPE AND DATES COVERED
		Final Report 7/1/89 - 12/31/93

4. TITLE AND SUBTITLE
Time Resolved X-Ray Detection

5. FUNDING NUMBERS
6835/00
61101E

6. AUTHOR(S)
Peter M. Rentzepis

7. PERFORMING ORGANIZATION NAME(S) AND ADDRESS(ES)
Univ of California, Irvine
Room 115, Administration Bldg.
Irvine, CA 92717-1875

8. PERFORMING ORGANIZATION REPORT NUMBER
AFOSR-TR- 94 0303

9. SPONSORING/MONITORING AGENCY NAME(S) AND ADDRESS(ES)
AFOSR/NC
Building 410, Bolling AFB DC
20332-6448

10. SPONSORING/MONITORING AGENCY REPORT NUMBER
F49620-89-C-0104

11. SUPPLEMENTARY NOTES

12a. DISTRIBUTION/AVAILABILITY STATEMENT
APPROVED FOR PUBLIC RELEASE; DISTRIBUTION IS UNLIMITED.

12b. DISTRIBUTION CODE

13. ABSTRACT *(Maximum 200 words)*

The goal of the project was to design, develop and construct an x-ray detector with high sensitivity and picosecond time resolution. This was achieved. A For Aerospace Charged Coupled Device, CCD, was utilized as the x-ray sensitive material around which the design and construction of the picosecond x-ray detector was built. this device has now become a commercial product sold, among other companies, by Photometrics Inc., and Princeton Research Inc. In addition we designed and built the first picosecond x-ray system. This system was utilized for the first ever picosecond x-ray diffraction experiments. The picosecond x-ray system was utilized in the oxidative fuel cell project to measure the decomposition of methanol and the change of the structure of its platinum catalyst. Another direct product of the work is the publication of 36 papers, in major scientific journals, and two patents.

14. SUBJECT TERMS

15. NUMBER OF PAGES
44

16. PRICE CODE

17. SECURITY CLASSIFICATION OF REPORT	18. SECURITY CLASSIFICATION OF THIS PAGE	19. SECURITY CLASSIFICATION OF ABSTRACT	20. LIMITATION OF ABSTRACT
UNCLASSIFIED	UNCLASSIFIED	UNCLASSIFIED	

NSN 7540-01-280-5500

Standard Form 298 (Rev 2-89)
Prescribed by ANSI Std Z39-18
298-102

PICOSECOND X-RAY DETECTOR

FINAL REPORT
April 20, 1994

Sponsored by
DARPA/AFOSR
Contract # F-49620-089-C-0104

Grantee

The Regents of the University of California
UCI, Irvine CA 92717

Principal Investigator: P. M. Rentzepis, UCI
(714) 856-5934

Table of Contents

Picosecond X-Ray Detector

I Executive Summary

The goal of the project was to design, develop and construct an x-ray detector with high sensitivity and picosecond time resolution. This was achieved:

A Ford Aerospace Charged Coupled Device, CCD, was utilized as the x-ray sensitive material around which the design and construction of the picosecond x-ray detector was built. This device has now become a commercial product sold, among other companies, by Photometrics Inc., and Princeton Research Inc.

In addition we designed and built the first picosecond x-ray system. This system was utilized for the first ever picosecond x-ray diffraction experiments. The picosecond x-ray system was utilized in the oxidative fuel cell project to measure the decomposition of methanol and the change of the structure of its platinum catalyst. Another direct product of the work is the publication of 36 papers, in major scientific journals, and two patents.

II. Introduction

X-ray diffraction is a well established field which provides the most detailed information on the molecular and crystal structure of materials. However the structure of the fast intermediate states and transient species produced during the interaction of materials with short laser pulses or other ultrafast phenomena have been studied in a very limited manner due to lack of short x-ray pulses with proper synchronization capability.

A considerable amount of ultrafast spectroscopy has been performed by means of picosecond and subpicosecond laser techniques. However, ultrafast optical spectroscopy is inherently incapable of providing the detailed information about material structures that can be obtained with x-ray diffraction methods.

X-ray pulses have been generated for several decades and pulsed x-ray sources have been also used to study the change in structure under various conditions [1-6]. Lately, synchrotrons have been employed to generate short x-ray pulses for time resolved x-ray experiments [4-6]. Synchrotron sources provide high intensity, tunable and highly collimated x-ray pulses with duration 100-200 ps, but are difficult to synchronize to external sources to an accuracy better than a few nanoseconds. X-rays produced by laser induced plasma provide another means for the generation of incoherent and coherent short pulse radiation, but most of the studies are confined to the soft x-ray region [7]. The conventional x-ray tube also has been modified to emit pulses in the millisecond range and flash x-ray techniques are capable of producing nanosecond pulses [1,2].

These devices which generate short x-ray pulses may be used in time-resolved x-ray diffraction research in areas such as lattice deformation by laser induced heating [5, 8], surface calorimetry [9], impact induced fast reactions processes [10], solid state decomposition, and explosion of energetic materials [11]. Each of the above techniques has advantages and disadvantages over the others depending on the specific application. For time-resolved studies such as

picosecond x-ray diffraction, a narrow linewidth is required. Sources with high flux of the characteristic x-ray radiation are preferred over other sources which generate x-rays with a broader spectrum. In order to achieve time-resolution on the picosecond scale in pump-probe type experiments, picosecond synchronization between the pump and probe sources is essential.

In this paper we report the details of a new technique for the generation of picosecond hard x-ray pulses, in the range 1-70 keV, at a high repetition rate and capable of accurate synchronization to other ultrafast sources. The basic idea revolves around the replacement of the cathode in a conventional x-ray diode with a photocathode excited by picosecond optical pulses [12].

III. Generation of Short X-Ray Pulses

Picosecond x-ray pulses provide an excellent means for basic research studies in time resolved structural changes and find use in several technological applications. To develop those new technologies which are based on the interaction of matter with short laser pulses it is critically important to understand better the radiation-matter coupling and mechanism of energy transfer. Such knowledge will make possible the evaluation and properties of the materials which will be suitable for new technological applications.

Time-resolved studies of fast phenomena have been accomplished by several techniques. Some of the most important include optical probing(absorption, and reflection), photocunductivity, time of flight mass spectrometry, and electron and x-ray diffraction. All of these techniques provide limited structural information and each has its own limits with regard to materials and processes. X-ray diffraction has been used for many years to study the structural properties of crystalline and to some extent amorphous materials on the atomic scale. One of the basic advantages of x-ray diffraction is that to a large extent x-rays interact weakly with matter and therefore provide an ideal, non-destructive, probe for structural studies of bulk as well of surfaces. Time-resolved x-ray diffraction studies have been demonstrated in recent years using short x-ray pulses produced by laser plasma or synchrotrons [1-7]. Most of the time resolved experimental measurements have been used for the study of the liquid-solid interface overheating and under cooling in silicon and germanium single crystals induced by pulsed laser irradiation. Nanosecond time resolution has been achieved by the employment of picosecond x-ray pulses from

synchrotron sources. Sub-nanosecond resolution has been achieved in x-ray diffraction experiments using laser produced plasma as a x-ray source [6,7].

Increasing the time resolution of x-ray diffraction measurements by moving into picosecond and subpicosecond time scales is important both from the fundamental physics and applied technology points of view.

From scientific point of view heating a solid material with ultrashort pulses produces non-equilibrium conditions between electrons and lattice for times less than the electron energy relaxation time. (When the electron system relaxation time is shorter than several picoseconds. The heat transport in an non-equilibrium electron-lattice system is also not well understood.)

From the applied point of view, interaction of materials with ultrashort laser pulses is the basis for rapidly developing new technologies, such as thin film processing. Additionally, the utilization of transient states of atomic and molecular systems are opening new fields for many technological advances in fields such as lithography, photochemistry and imaging.

Picosecond time-resolved studies of transient phenomena by x-ray diffraction have been absent due to difficulties of: 1) production of narrow linewidth picosecond x-ray pulses and 2) synchronization of the pump sources with the picosecond x-ray generator with picosecond accuracy .

We now present our new technique for the generation of picosecond hard x-ray pulses, which can be synchronized with other fast sources with picosecond accuracy [8,9]. The picosecond x-ray pulses are generated in an x-ray diode where the photocathode electrons are emitted by ultrashort laser pulses.

IV. Picosecond X-Ray Diode

IVa. Design Considerations

In conventional x-ray tubes anode current generation of the order of tens of miliamps is attainable. Modulation of the x-ray output is possible either by modulation of the anode voltage or cathode emission. The x-ray diodes using thermionic emission as the electron source have a long response time, while x-ray flash tubes can produce much shorter pulses by employment of cold cathodes. In a flash x-ray diode a vacuum discharge is initiated by field emission, plasma growth or microparticles [10]. In such systems pulses of tens of nanoseconds in duration or longer are produced. Replacement of the cathode in the x-ray diode by a photocathode excited by short laser pulse allows for picosecond x-ray

generation. The duration of the x-ray pulse produced by a diode is determined by the duration of the electron pulse impinging on the anode. Therefore in order to evaluate the operation of the x-ray photodiode we consider the generation of short electron pulses on the cathode and their (changes during) propagation between the cathode and anode. In order to obtain enough x-ray flux to be detected and for use in diffraction and other time resolve experiments in high peak current electron pulses have to be generated and subsequently propagated through the x-ray diode.

In the last few years photocathodes using short pulse laser excitation have received great attention as a source for high current and short duration electron pulses[11-13]. This interest is related to the application of these types of electron sources as free electron lasers and acceleration injectors. Some of the most important photocathode requirements include the production of electron pulses of high peak current densities (kA/cm^2) and picosecond duration. Metallic photocathodes due to their excellent electric and heat conductivity properties and higher damage threshold are preferable to semiconductor or alkali-metal composites. Additionally the composite photocathodes demand pressure below 10^{-9} Torr, while pure metal photocathodes require little preparation and a modest vacuum [below 10^{-6} Torr], with virtually unlimited lifetime and easy restoration by cleaning and polishing. The main disadvantage of a metallic photocathode is its low quantum efficiency and high work function which require intense, deep ultraviolet light (UV) for sufficient electron photoemission. Recently new results have been reported regarding the photoionization properties of metals for laser driven metal photocathodes [11,14].

We have carried out a comparative study of several metals as possible photocathode materials to be used in a x-ray source system. The details of this study were reported elsewhere [14] and here the results are only summarized in Table I. Two wavelengths (263 nm and 211 nm) have been used for all metals and only for Al we have measured the quantum efficiency at 193 nm. In Table I the experimental data, reported in the literature which is relevant to our experiments are also presented.

The operation of the x-ray diode with a photocathode is otherwise similar to those found in a conventional tube where the output x-ray spectrum is determined by the anode material and electron energy. In order to evaluate the performance of a photo-excited x-ray diode we follow the analysis of a space-charge limited photodiode as reported in reference [13]. For simplicity we

consider a planar x-ray diode consisting of a flat photocathode and a flat anode separated by a fixed distance in vacuum (Fig.1). In a planar diode, the total charge per unit electrode area traveling from cathode to anode through free space and the electric circuit is:

$q_t(t) = q_c(t) + q_i(t)$

where q_c is the capacitive charge per unit area and q_i is the induced charge component from electron motion [13]. Before light strikes the cathode there is no current in the circuit and therefore $q_i = 0$. The charge after illumination available is the capacitive charge which has a static origin. If the voltage applied between electrodes is V, the available charge is:

$q_c = C_s V$

where C_s is the diode capacity per unit area. For a plane diode: $C_s = e_0/d$, where d is the anode-cathode separation and e_0 is the free space permittivity. For a practical device the anode-cathode distances should be in the range of 5 - 30 mm and the applied voltage below 500 kV. In this case, both relativistic effects as well as field effects may be justifiably neglected.

A diode having the described geometry and excited by picosecond light pulses normally operate in the transient or pulsed mode. In the transient regime, the duration of the electron pulse (t_p), traveling from the cathode to the anode is shorter than the transit time of the electrons between electrodes. The transit time of non-relativistic electrons across the diode gap is given by:

$t_t = 1.5\ (2m/e)^{1/2}\ d/V^{1/2}$

where e and m are the charge and mass of the electron, respectively [13].

When all the available capacitive charge q_c has been emitted, the intensity of the electric field at the cathode goes to zero owing to charge screening. Additional photons generate electrons at the surface in a roughly zero field environment that mostly results in excess electrons returning to the cathode. Thus when the cathode is illuminated by an intense short light pulse, only the capacitive charge q_c can be extracted. If the time between successive light pulses striking the cathode is longer than the transit time t_t, then only one electron pulse is present in the diode gap at a time and the induced charge density is therefore zero. The maximum peak current density at the anode is then:

$J_M = q_c/t_a$

where t_a is the electron pulse duration at the anode which is directly related to the light pulse width t_p. It is a fair assumption that the electron pulse formed at the cathode surface by photoemission initially has the same duration as the

incident picosecond laser pulse. However, space charge interaction within the electron pulse during propagation between cathode and anode may result in significant temporal and spatial dispersion, depending on the initial current density of the photoelectron burst. Coulomb repulsion between the electrons inside the pulse is primarily responsible for a longer temporal duration and wider spatial distribution of the electron pulse at the anode.

The duration t_x, of the x-ray pulse generated by electron impact on the anode is assumed to be equal to the duration of the electron pulse at the anode, $t_a = t_x$. Therefore, spatial distribution of the x-rays on the anode surface are largely determined by the final distribution of the electrons at the anode. Computer simulations of the temporal dispersion of short electron pulses traveling across a diode have been reported previously [15]. It has been shown that widening of the electron pulse duration at the anode may increase significantly when very short electron pulses are generated at the cathode and the diode is operated at the space-charge limit. In Fig. 2 we present the calculated pulse duration at the anode for space charge regime of operation of a plane diode with 10 mm cathode-anode separation and an applied voltage of 75 kV [15].

The transient mode of operation of the diode allows for much higher peak current densities in comparison to steady-state operation. In the steady-state regime of operation the space-charge limited current density in the diode is then governed by the well-known Langmuir-Child equation:

$$J_L = e_0 (32e/81m)^{1/2} V^{3/2}/d^2$$

Consequently one may also expect higher peak x-ray intensities in the pulsed mode of operation, which scales as $\sim t_t/t_a$.

The spectral properties, spatial distribution and efficiency of x-ray radiation production by electron bombardment has been studied in detail [16]. When narrow linewidth characteristic radiation is required anodes made from light elements are preferable. When continuum radiation is desirable heavier elements are usually employed as anodes. We note that characteristic radiation has an isotropic angular distribution, while bremsstrahlung becomes more peaked in the forward direction and depleted in the backward direction as the incident electron energy increases. Depending on the needed properties of the x-ray radiation the proper design considerations have to be carried out which will tend to maximize the usable x-ray output [17].

IVIb. X-Ray Photodiode

In the present experiment a copper anode was used to produce Ka radiation with l= 1.54 A and Dl/l = 2.9×10^{-4}. Using the data for production Ka radiation efficiency from thick targets of pure elements presented in [17,18] and the above analysis we have estimated the output of such a pulsed x-ray diode with 1 cm anode cathode separation at various applied voltages. The results are given in Table II. For Copper Ka production the optimum voltage is about 300 kV [17].

A polished aluminum flat cathode was used in the experiment has a quantum efficiency of 4.65×10^{-6} for 193 nm radiation (Table I). For an applied voltage of 75 kV and 1 cm anode cathode gap the maximum available charge per mm^2 is 66.4 pC. This amount of charge will produce 4.97×10^5 Cu Ka photons per pulse per unit solid angle. Taking into account the quantum efficiency of the Al cathode we find that 92 $\mu J/cm^2$ per pulse of UV radiation at 193 nm are required to extract all available charge. At a pulse repetition rate of 300 Hz this corresponds to an average power density of 27.6 mW/cm^2.

In order to increase the usable x-ray output, a more sophisticated geometry of anode-cathode system is now under evaluation. The diode consists of anode in the form of a small angle cone inserted in a cathode which is in a form which is expected to maximize the laser pulse effective electron photoemission. This geometry is expected to increase considerably the x-ray flux within the 10∞ take off angle. An additional increase in the x-ray flux is expected by increasing the applied voltage from 70 KV to 250 KV. This is a feasible task facilitated by the availability of pulsed transformers which operate at high repetition rates, due to the low power load required in our experimental system. Utilization of the picosecond pulsed time resolved x-ray diffraction experiments has been presented briefly (ref. 9) and will be described in detail in a forthcoming communication. Increasing the applied voltage to several hundred kilovolts is feasible by using pulse transformers which can operate at high repetition rate, since the average power load is low.

V. Laser System

IVa. Generation of intense 193 nm picosecond pulses

In order to meet the above requirements for the UV pump source that drives the x-ray diode, a high power picosecond laser system based on an ArF excimer amplifier has been developed that generates UV pulses with duration shorter than 10 ps, and pulse energy up to 2.5 mJ at a repetition rate of 300 Hz. The experimental system is shown in Fig. 3. A detailed description of the system is presented in [19] and therefore only brief outline will be given here.

The master oscillator is a cw mode-locked Nd:YLF laser generating 50 ps duration pulses at 1053 nm and 76 MHz repetition rate with an average power of 13 W. Its output is up-converted by a LBO crystal to 2 W of 527 nm radiation which is used for synchronous pumping of a single jet dye laser. The pulse duration of the dye laser was found to be 5 ps with an average output power of 200 mW at 724 nm. Part of the remaining unconverted 1053 nm radiation from the LBO crystal is used to seed a Nd:YLF regenerative amplifier which produces 50 ps pulses with energy of 1.5 mJ at a 300 Hz repetition rate. The output of the regenerative amplifier is converted to second and fourth harmonics in a series of two BBO crystals. The 527 nm radiation remaining after the fourth harmonic crystal is used to pump a two-stage dye amplifier. The 263 nm pulse energy is limited to the 100-200 mJ range by detuning the fourth harmonic crystal away from optimum phase matching. Thus the amplified dye laser pulse energy is in the range of 10-15 mJ.

The 193 nm seed pulses were generated in another BBO crystal by mixing 263 nm and 724 nm pulses. Selecting a proper BBO crystal made possible to generate steady seed pulses with energies of 1.5-4 mJ at 300 Hz. The seed pulses at 193 nm were amplified in a double pass ArF amplifier to an energy of 2-2.5 mJ, thus an average output power of 600-750 mW was obtained. Streak camera measurements of the amplified 193 nm pulses gave an upper limit of 9 ps (Full Width at Half Maximum) for the pulse duration.

The operation of the system is critically dependent on the synchronization of various components. The electronic components used for synchronization are also shown in Fig. 3. Given that this Nd:YLF regenerative amplifier possesses a different cavity round-trip time than the master cw mode-locked laser, the number of passes inside the regenerative amplifier must be fixed. The 38 MHz RF signal from the mode-locker of the master oscillator is used for timing the pulse selection and switch out signals for the Pockels cell in the regenerative amplifier, which subsequently triggers a digital delay pulse generator. The delay generator thus becomes a timing source for the ArF discharge, streak camera

sweep, etc. A zero drift control module was used to limit the jitter in the gain timing of the excimer discharge to ± 2 ns. Such fluctuations in the discharge timing are tolerable given a seed pulse transit time through the amplifier of 7 ns and a discharge gain lifetime greater than 10 ns. The pulse-to-pulse intensity fluctuation under normal operating conditions depends on many factors, including gas lifetime and discharge parameters, but was typically less than 30% with a fresh gas fill. The ArF amplifier was equipped with a liquid nitrogen gas purifier which allowed for up to 4 hours operation with a single gas fill and less than 50% degradation of the output power at a fixed discharge high voltage. It is noteworthy to consider that at a 300 Hz repetition rate more than 10^6 pulses are amplified per hour. In this system picosecond pulses of several optical wavelengths (1053 nm, 724 nm, 527 nm, 263 nm and 193 nm) are synchronized with the x-ray pulse to picosecond accuracy.

Vb. Generation of picosecond x-ray pulses.

The output radiation from the ArF excimer amplifier was used to operate the x-ray diode shown in Fig.1. The cathode and the anode were made from bulk samples of Al and Cu, respectively, and polished using Micro-Mesh® abrasives to achieve a surface roughness of less than 25 mm. The electrodes were cleaned with hexane and installed in the vacuum chamber. The flat surfaces of the anode (3 mm diameter) and cathode (12 mm diameter) were separated by 10 mm. The x-ray diode chamber was normally kept at pressure of 4-7 x 10^{-9} Torr. The UV radiation was directed on the cathode through a MgF_2 window at 15° relative to the normal of the cathode surface. The diode chamber was equipped with two 250 mm thick Be windows for the x-ray output. One arm of the x-ray output impinges upon the entrance slit of a streak camera used for pump/probe timing and pulse duration measurements. The measured pulse duration of the amplified 193 nm pulse was found to be 9 ps (FWHM), which is much less than the 190 ps electron transit time calculated for this x-ray diode [13]. Also a repetition rate of 300 Hz implies a period of 3.3 ms between UV pulses so that the electron pulses in the diode do not overlap in time. Therefore the amount of Cu K_a x-ray photons produced by each UV pulse can be evaluated individually. At 70 kV anode-cathode voltage, the maximum amount of charge density which can be extracted from the cathode is 4.9 x 10^{-11} C/mm^2, which yields 3 x 10^8 electrons per pulse. Incorporating the efficiency of K_a production from a Cu

target into the quantum yield calculation [18] results in 3.7×10^5 photons of Cu K_a radiation being produced per unit solid angle per pulse.

Temporal measurements of the x-ray output were carried out with a high repetition rate, picosecond resolution streak camera (Kentech Instruments Ltd. 10 ps resolution used in the measurements) [20]. The photocathode of the camera was divided into two sections: a quartz window coated with 30 nm gold film sensitive to 193 nm radiation and 1.5 mm mylar film coated with 30 nm thick low density CsI sensitive to x-ray photons. The streak camera output was optically coupled to a Hamamatsu Saticon CCD camera coupled to an electrostatic image intensifier. The output of the CCD camera is stored on a Hamamatsu video processor for measurements and enhancement. Unfortunately, the x-ray intensity output was insufficient for single shot measurements, and frame accumulation of several thousand shots was necessary to obtain a measurable signal. Two different trigger sources were employed to trigger the streak camera sweep: an additional channel from the same digital delay generator used to trigger the excimer amplifier, or the output of a fast vacuum photodiode illuminated by second harmonic pulses. Although in both cases successful measurements were performed, the jitter using the photodiode trigger was less and for this reason it was used for the x-ray pulse duration measurements. An estimate of the effect of timing jitter on pulsewidth measurements must be included in an attempt to derive an actual pulsewidth from streak camera observations. In order to estimate the jitter, the UV intensity incident on the streak camera slits was attenuated so that a UV pulse image was accumulated by the same number of frames (~2000) as the x-ray image. Images of both x-ray and UV pulses were recorded simultaneously. Scans of this image in the videoprocessor, result in a UV image duration of 50 ps (FWHM) and a x-ray pulse shape width of 130 ps (FWHM). The amplified 193 nm pulsewidth is known to be less than 9 ps (FWHM) from previous measurements [19]. Scaling the x-ray measurement by the ratio of the known/observed UV pulsewidths in order to account for the effects of timing jitter gives a lower limit for the x-ray pulse duration of 20 ps. If the jitter broadens the observed pulse duration in a cumulative manner, then subtracting the difference of the UV pulsewidths from the observed x-ray signal may be a more appropriate adjustment that gives an upper limit for the x-ray pulsewidth of 90 ps. In any case, it is safe to assume that the true x-ray pulse duration lies in the range of 20-90 ps. Using computer simulation data for the dispersion of short electron pulses across a diode in the

space-charge regime, it is estimated that a 9 ps electron pulse at the cathode surface yields a 23 ps electron pulse at the anode [15]. This value is in agreement with the measured x-ray pulse duration, assuming that the x-ray pulsewidth equals the electron pulse duration at the anode.

VI. X-Ray Detection System

The x-ray output from the diode through the other Be window was used to carry out spectral and time-resolved x-ray diffraction measurements. The UV beam from the excimer amplifier was attenuated and focused with 1 m focal length lens onto the cathode surface. The UV spot on the cathode was approximately 3 mm diameter and situated opposite the anode. No detailed study of the influence of the size and position of the UV beam on the cathode on the x-ray output was carried out. However shifting the position of the UV spot on the cathode changed the distribution of the x-ray production from the anode surface. Pinhole pictures suggest that for the above positioning of the UV beam the predominant part of the x-ray output was generated on the flat surface of the anode. Fig. 4 shows a pinhole image of the spatial x-ray distribution on the anode surface. It is noteworthy that the use of a photocathode allows, in principle, the implementation of more complicated geometry's for varying the spatial and temporal distribution from the x-ray source.

The x-ray output was measured using a large area CCD camera designed specifically for direct x-ray imaging. The camera consists of a Ford Aerospace 2048 x 2048 MPP CCD chip (15 mm pixel), cooled by liquid nitrogen (Photometrics Ltd.), and interfaced to a Macintosh IIfx computer [8]. The active area of the CCD is 30 x 30 mm^2, and the conversion efficiency for 8 keV photons is about 15%. Cooling to low temperatures (-100°C) reduces the dark current to allow for single photon detection. Camera readout at 50 kHz with 4 x 4 pixel binning was usually employed to increase the data acquisition rate, since the full 15 mm spatial resolution was seldom required.

The measured x-ray output flux at 40 cm from the anode and a 10° take-off angle was 3×10^4 Cu K_a photons per cm^2 per second. This observed value was in good agreement with the calculated value for a pulsed x-ray diode with a saturated photocathode. Single or double crystal monochromator arrangements yielded ~3% Bragg reflection from a Si (111) crystal and about 6% Bragg reflection from Pt (111) crystal. The measured ratio of intensities of the

K_{a1}, K_{a2} and K_b lines correspond to the output from a conventional x-ray tube [16]. Fig. 5 shows the dependence of Cu K_a output on the applied voltage at constant UV illumination. The output increases slightly faster than $(V/V_K - 1)^{1.67}$ due to the dependence of the available charge on the applied voltage (V_K represents the K-shell ionization voltage of the anode material) [16]. When the x-ray diode was operated in the saturated mode the fluctuations of the x-ray output energy was found to be an order of magnitude less than the fluctuations in the input UV pulse energy which is a rather expected result.

The estimated energy required of this system for the conversion to 193 nm radiation to Cu K_a radiation is approximately 0.5% of the UV flux necessary to saturate the x-ray photodiode.

An estimate of the effect of timing jitter on pulsewidth measurements must be included in an attempt to derive an actual pulsewidth from the streak camera observations. In order to estimate the jitter, the UV intensity incident on the streak camera slits was attenuated so that a UV pulse image was accumulated in the same number of frames (~2000) as a typical x-ray image. Fig. 6a is a photograph of the streak camera image of two UV pulses separated by 500 ps and the x-ray pulse image from 2000 frames of integration. It should be noted that this image was deliberately overexposed to enhance the contrast for photographic reproduction. Scans of this image in the videoprocessor provide a measurement of the UV pulse duration of 51 ps (FWHM) as shown in Fig. 6b. This figure also shows the x-ray pulse shape with an observed duration of 128 ps (FWHM). The amplified 193 nm pulsewidth is known to be less than 9 ps (FWHM) from previous measurements [19]. Scaling the x-ray measurement by the ratio of the known/observed UV pulsewidths in order to account for the effects of timing jitter gives a lower limit for the x-ray pulse duration of 20 ps. If the jitter broadens the observed pulse duration in a cumulative manner, then subtracting the difference of the UV pulsewidths from the observed x-ray signal may be a more appropriate adjustment that gives an upper limit for the x-ray pulsewidth of 90 ps. In any case, it is safe to assume the true x-ray pulse duration lies in the range of 20-90 ps. Using computer simulation data for the dispersion of short electron pulses across a diode in the space-charge regime, it is estimated that a 9 ps electron pulse at the cathode surface yields a 23 ps electron pulse at the anode [15]. This value is in agreement with the measured x-ray pulse duration, given the validity of the assumption that the x-ray pulsewidth equals the electron pulse duration at the anode.

VII. Applications to Picosecond X-Ray Diffraction

VIIa. Intermediate Structures in Pt.

The output from the x-ray diode was used to perform for the first time picosecond time-resolved x-ray diffraction experiments. The goal of the experiment was to observe crystal lattice distortion due to picosecond light pulse heating. A platinum (111) crystal was placed on a three-axis Eulerian cradle [illegible] cm from the anode of the x-ray diode. Two 0.5 mm parallel slits were mount between the x-ray source and the Pt crystal to collimate the x-ray beam. The x-ray pulse impinged upon the sample at an angle of 19.87° (Bragg condition). The crystal dimensions (1 mm thick and 9 mm in diameter) allow the CCD camera to record the diffracted x-rays along the whole diameter of the crystal.

The output of the ArF amplifier was split in two arms, one used to drive the x-ray diode, and the other to heat the Pt crystal after a proper delay was inserted. The UV heating (pump) beam was focused on the crystal surface in a 2 mm diameter spot with approximately 1.5 mJ/cm^2 average energy density per pulse. Under such conditions no surface damage was observed even after many hours of irradiation. The timing between the heating pulse and the x-ray pulse was measured using the streak camera as discussed above.

Fig. 7 shows a typical picture from the CCD detection system. With proper alignment the diffraction from the whole crystal is recorded. A metal screen positioned on the crystal surface divided the crystal into two segments, the lower section where the heating UV radiation was directed and an upper area not illuminated by the UV radiation during all measurements. The results reported here were produced by thirty minute exposures (5.4×10^5 shots), and the signal from the upper part of the crystal was used as a reference in order to account for variations in the x-ray flux. Typically two consecutive exposures are made, one with UV radiation heating the lower part of the crystal, the next one without UV heating. Fig. 8 is an example of the horizontal scan of such exposure averaging 20 pixels in the vertical direction (1.2 mm on CCD). Fig. 8 depicts the reference signals (a) and (c), as well as the diffracted x-ray photons detected from the unheated (b) and heated (d) areas of the crystal. The decrease in intensity of the diffracted signal due to the heating is readily seen. The maximum decrease in the diffracted x-ray signal due to laser pulse heating was ~6% with the delay

between the UV heating pulse and the probe x-ray pulse set at less than 100 ps. Within this experimental arrangement, the timing accuracy of the arrival of the pump and probe pulses at the sample was about 100 ps. When the delay of the x-ray pulse was increased to 400 ps relative to the maximum interaction, the diffracted signal decreased to 2-3%, which was within the fluctuation of the measurements.

Temperature changes in the crystal due to laser heating affect the diffracted x-ray by thermal strain which alters the lattice spacing and the thermal-ionic motion which decreases the scattering power (Debye-Waller effect) [22]. These effects have been treated in detail only for a constant and homogeneous temperature distribution. A recent report [23] considering a short pulse laser heating on metals has shown that for 10 ps heating laser pulse the temperature distribution in the metal is temporally and spatially inhomogeneous. The penetration depth of the x-ray beam in the Pt sample is estimated to be about 600 nm compared to about 20 nm for the absorption length of the 193 nm radiation. Thus caution should be exercised when applying the standard expression for the estimation of the influence of the heating on diffracted x-ray signals. From these measurements we estimate that the temperature of the surface of the crystal was increased by 100-300 $^{\circ}$C as a result of the picosecond laser pulse heating. More detailed measurements and discussion will be presented in a subsequent communications.

VIIb. Transient structures in Au (111) Crystal.

Using 10 ps, 193 nm pulses to generate characteristic Cu Kα picosecond x-ray pulses, $\tau < 50$ps, at 300Hz, we have being able to detect, for the first time ever, transient lattice spacing in gold crystals.

The application of short laser pulses to nanostructure fabrication is a rather new and fast growing area of research. Because it is now possible to control precisely the location and amount of energy delivered as well as to realize high heating/cooling rates, short pulse laser heating makes an important contribution to the development of new means for material processing in microelectronics [24]. Understanding the mechanism responsible for heat transfer during short pulse laser heating is essential for the further improvement of these technologies [25]. So far most of the experimental results related to time resolved heat transfer studies have been carried out by reflectivity measurements. In these experiments the electron gas temperature is measured and based on this data deductions are made about lattice temperature [24-27].

Direct measurements of the lattice temperature are obviously necessary for the understanding of the complete mechanism of heat transfer. Time resolved electron and x-ray diffraction are the most useful techniques for the measurement of the lattice behavior during pulse laser heating. Picosecond time resolution has been achieved in electron diffraction experiments from thin crystals [28,29] and nanosecond resolution experiments have been reported in x-ray diffraction measurements on silicon during pulse laser annealing [30]. Subnanosecond resolution has also been achieved with a laser plasma x-ray source using an x-ray streak camera to study the shock wave propagation in crystals under picosecond laser illumination [31].

Recently we have develop a new system for time resolved x-ray diffraction measurements [32,33]. The system is based on application of ultraviolet (UV) picosecond pulses for generation of highly synchronized picosecond electron and x-ray pulses. In this letter we report the results of the application of this system to time resolved picosecond x-ray diffraction measurements on a thin gold crystal heated by 193 nm, picosecond pulses. The experimental system has been described in detail elsewhere [34,35] and here only

its characteristics related to the time resolved x-ray diffraction will be summarized. A cw mode-locked Nd:YLF laser is used as a master-oscillator/clock in a laser system which produces 10 ps, 193 nm pulses with energy up to 2 mJ and 300 Hz repetition rate determined by the ArF excimer amplifier. The UV pulses are split in two beams, one is used to drive an x-ray photodiode and the other as a pump pulse to heat the gold crystal. Picosecond Cu Ka x-ray pulses are generated in an x-ray photodiode by illuminating an Al photocathode with picosecond 193 nm pulses. The electron pulses from the cathode are accelerated by a 70 kV dc electric field and impinge on a cooper anode to produce x-ray radiation. When 10 ps UV pulses are used to illuminate the photocathode they produce electron pulses with the same duration near the cathode surface, however due to space charge effects in the diode the pulse duration will increase by the time it arrives at the anode[35,]Using the approach reported in [36] we have calculated that for our diode the electron pulse duration at the anode will be 21 ps, which we accept as a lower limit. Since we did not have the capability to measure the duration of a single x-ray pulse, we relied on accumulative measurement of several thousands pulses with a high repetition rate x-ray streak camera. By this means we have estimated that the upper limit of the x-ray pulses used in our experiment to be 50 ps. Two vertical slits 25x0.5 mm^2 and 25x0.25 mm^2 separated by 30 cm were used to define the x-ray beam to be diffracted from the (111) gold crystal. The distance between the x-ray diode and the gold crystal was 40 cm, which gave for 10^o take off angle about $4x10^4$ Cu Ka photons per cm^2 per second on the crystal.

Picosecond 193 nm pulses were used to heat the crystal. The pulses passed through a variable delay and then were focused with a 35 cm focal length lens which made a spot size of about 3 mm diameter on the crystal. In order to facilitate the overlap alignment of the x-ray and UV beams a small area of the Au crystal was evaporated by focusing the laser beam (see Fig.9). The Bragg angle for 1.54 A radiation for Au(111) crystal is 19.086^o and the incident x-ray radiation on the crystal surface covered a strip ~1.4 mm wide. The 150 nm thick gold crystal had a 9 x 15 mm^2 surface area and was grown on 100 mm thick mica crystal. The crystal was placed on a three axis Eulerian cradle allowing for accurate alignment. The timing of the x-ray pulse and the UV pulse was achieved by a streak camera with a composite cathode sensitive to both x-ray and UV radiation. The streak camera used to measure the timing was situated at the opposite side of the x-ray chamber [33] and the timing of UV and x-ray pulses on

the crystal was geometrically translated. The estimated accuracy was better than 100 ps.

The diffracted x-ray radiation was detected by a large area CCD camera. The camera consists of a Ford Aerospace 2048x2048 MPP CCD chip (15 mm pixel), cooled by liquid nitrogen and interfaced to a Macintosh IIfx computer. The active area of the CCD is 30x30 mm^2, cooling the CCD to -100°C allows for a single x-ray photon detection. In the measurements reported here 4x4 or 4x2 pixel binning were employed for 1800 s exposures (5.4×10^5 shots). Fig. 1 shows a typical picture of the diffracted x-rays as displayed by the CCD detection system. The gap in the signal is due to the evaporated part of the crystal and the heating area is located just above this gap. The lower part of the crystal as well as its upper part were not illuminated with UV radiation during any measurement and were used only as reference. Typically, two consecutive picosecond x-ray exposures were made, one with UV radiation heating the selected part of the crystal and another without UV heating.

Heating solid materials with nanosecond and picosecond laser pulses, when the laser radiation induces neither melting nor vaporization has been studied theoretically in some detail [37]. Recent studies with femtosecond pulses [26] suggest that for gold films with thickness up to 300 nm the heat transport is very fast, hundreds of femtoseconds. Therefore in our experiment although the pulse duration of 10 ps is an order of magnitude [25] longer than the electron-phonon relaxation time, the film thickness is less than 300 nm and the fast heat transport will contribute to a much faster increase of the film temperature than the heat diffusion theory predicts. In Table III the optical and thermal properties of gold and mica which are relevant to our experiment are given. From those data we calculate that for a laser pulse, t_p = 10 ps, the diffusion length is $(2kt_p/C_pr)^{1/2}$ = 51 nm. This length represents the crystal depth heated during the pulse illumination. Additionally it takes about 80 ps for the heat to diffuse through the crystal to the mica substrate. Using the heat propagation speed in gold films reported by Brorson et al. [26] we find that only ~0.2 ps are necessary for the heat to spread through the 150 nm thick gold film.

In our experiments the 193 nm pulse energy transferred on to the gold sample was less than 0.15 mJ and for a spot diameter of ~3 mm the maximum energy density was 2.1 mJ/cm^2. The spatial distribution of the intensity in the cross section of the 193 nm beam was a flat top with uniform intensity of about 80%. Rough estimates [38] show that a pulse energy of 0.1 mJ will increase the

temperature of the heated area of the gold crystal by about 90°C. After about 100 ps, according to heat diffusion theory, the absorbed energy will be distributed in the crystal volume of 3 mm diameter and 150 nm thickness. The heat dissipation from this area may take three directions - along the gold film, by the air and through the mica substrate. Estimates have shown that at least in the nanosecond time frame heat dissipation takes place mostly through the mica substrate and after 10 ns the temperature of the gold film will drop by about 20%.

In our experiments we have measured the x-ray diffraction intensity as a function of time delay between the UV pump and x-ray probe pulse from -100 ps to +1.8 ns.

Temperature changes in a crystal are expected to affect the scattered x-rays in two ways:

1) Thermal ionic motion which will decrease the height of the Bragg peak intensity (Debye-Waller effect).

2) The thermal expansion which will result in the increase of the lattice spacing and thus change the Bragg angle for coherent scattering, resulting in a "shift" of the Bragg diffracted band.

To our knowledge the problem of x-ray scattering from heated crystals taking into account both of the above mentioned effects together has not been sufficiently studied [39]. Therefore we estimate each effect separately.

Using the Debye-Waller factor data for gold crystal [40] we find that for a uniform lattice temperature increase of 100°C, above room temperature, the decrease in the scattered x-ray intensity of the Bragg peak will be about 2%, correspondingly, for a temperature change of 200°C the intensity will decrease by 5%. In Fig. 10 the ratio of the scattered x-ray intensities for cold and heated crystal samples are presented. For negative delays, that means the x-ray probe pulse reaches the crystal before the UV pulse, the ratio is 1. When the x-ray probe pulse arrives after the UV heating pulse the ratio drops to about 0.90 and stays on that level for the maximum delay, 1.8 ns, used in our experiments. The measurements were carried out with the maximum energy per pulse available to us. For the experiments presented here the pump pulse energy delivered to the crystal was in the range 80 -150 mJ. For every exposure the pump pulse energy was monitored by an oscilloscope, however no recording of the energy of every single pump pulse was available. It is possible that some pulses have higher or lower energy due to temporal fluctuations mainly in triggering the excimer amplifier. We estimate that the fluctuation in the output pulse energy could be as

high as 30%. Although the fluctuations in the signal are comparable to the x-ray intensity changes observed, the recorded decrease in the scattered x-ray intensity was consistently higher than the one which the Debye-Waller theory predicts. The same behavior has been observed in cw heating experiments [39]

Assuming a uniform lattice temperature increase of 100°C and the linear thermal expansion coefficient given in Table III we calculate that the change in the Bragg angle will be 0.03 arc degrees. This value in our experimental set up, translates to a shift of 2 pixels on the CCD. For 200°C temperature change the shift will be 4 pixels. In the measurements presented 4x2 binning of the CCD was used, binning by 2 was in the direction of the Bragg angle (horizontal axis of Fig. 9,11). In Fig. 11a we show a comparison of the x-ray diffraction data obtained for the heated and unheated areas of the gold crystal. The signal is averaged over 20 pixels along the vertical axis and scanned along the horizontal axis (see Fig. 9). In Fig. 11b we show the scans of the same two x-ray exposures but from the area on the crystal where no heating was applied. In all measurements comparisons were made, as shown in Fig. 11b, with signals above and below the heated area of the crystal. A 2 to 4 pixels shift in the Bragg angle was clearly observed after heating. For negative time delays no such shift in the heated area was recorded. As expected the shift was found to be related to the heating pulse energy and for pulse energies below 0.03 mJ no shift was observed.

Both effects, decrease in the scattered x-ray intensity and shift in the Bragg angle, were clearly detected. A detail study on the dependence of the diffracted intensity decrease and shift on the heating pulse energy were not made because of the limited pump pulse energy available. In both signals the transition region near the zero time delay was clearly observed as shown in Fig.10. However because of our time resolution of 50 ps, which is essentially the time required for diffusive temperature equilibrium in the 150 nm thick gold film it was difficult to achieve a better resolution in this transition region. We hope that with an additional regenerative amplifier, now under construction, and shorter x-ray pulses we will be able to resolve better this transition in time and energy.

In summary we have developed an experimental system for time resolved x-ray diffraction studies which has a resolution of better than 50 ps. The system has been applied as an ultrafast lattice temperature probe during picosecond laser heating of gold (111) crystals. The system is under further development to reduce the optical pulse below 1 ps which will allow for generation of x-ray pulses shorter than 10 ps without sacrifice in the number of x-ray photons

generated per pulse. Additionally, our planned increase in photon flux, better stabilization and monitoring of the pump pulse energy, will greatly increase the uses of this experimental system.

VIII. Summary and future developments.

The results presented show that an optically driven x-ray diode is capable of generating high repetition rate hard x-ray pulses in the range of 10-100 ps. Replacement of the anode material allows a wide spectral range of characteristic wavelengths to be generated. At 70 kV the estimated brilliance is about 300 kW/mm^2, which is several orders of magnitude higher than the conventional x-ray tube. However, in spite of the gain in peak power, the amount of K_a x-ray photons per pulse in a small solid angle required for time-resolved diffraction is too low for single shot measurements. For most practical cases, accumulation of thousands of shots is necessary to produce reliable results. In order to preserve the picosecond time resolution of the measurements, low jitter between the x-ray probe pulse and the pump source must be maintained. As mentioned above, this system provides picosecond pulses at several wavelengths which are accurately synchronized with the x-ray pulse; while for synchronization to other ultrafast sources, the RF signal of the cw mode-locked oscillator makes a an excellent system clock. The observed jitter between the x-ray pulse and the output from the delay generator was approximately 200 ps using the RF signal as the trigger source (Fig. 11).

The low duty cycle of this system is determined by the 300 Hz repetition rate of ArF excimer amplifier. Existing laser technology will allow the production of powerful UV pulses at higher repetition rates, i.e., several KHz with pulse durations in the picosecond and subpicosecond range, which may be exploited for further development of this technique for the generation of x-ray pulses shorter than 10 ps.

IX. References

1. J. G. Lunney, P. J. Dobson, J.D. Hares, S.D. Tabatabaei, and R. W. Eason, Opt. Commun. **58**, 269 (1986).
2. B. C. Larson and J. Z. Tischler, SPIE **1345**, 90 (1990).
3. B. C. Larson, J. Z. Tischler and D. M. Mills, J. Mater. Res. **1**, 144 (1986).
4. S. Kojima, I. Maekawa, S. Kawado, T. Takahashi, T. Ishikawa, and S. Kikuta, Rev. Sci. Instrum. **63**, 1164 (1992).
5. J. R. Bushchert, J. Z. Tischler, D. M. Mills, Q. Zhao, and R. Colella, J. Appl. Phys. **66**, 3523 (1989).
6. J. S. Wark, D. Riley, N. C. Woolsey, G. Keihnand, and R. R. Whitlock, J. Appl. Phys., **68**, 4531 (1990).
7. N. C. Woolsy, J. S. Wark and D. Riley, J. Appl. Cryst. **23**, 441 (1990).
8. B. Van Wonterghem and P. M. Rentzepis, SPIE **1204**, 784 (1990).
9. T. Anderson, I. V. Tomov and P. M. Rentzepis, J. Chem. Phys. (to be published).
10. R. Germer, J.Phys. E: Sci. Instrum. **12**, 336 (1979).
11. T. Srinivasan-Rao, J. Fisher, and T. Tsang, J. Appl. Phys. **69**, 3291 (1991).
12. D. Charalambis, E. Hontzopoulos and C. Fotakis, J. Appl. Phys. **65**, 2843 ((1989).
13. J. P. Girardeau-Montaut and C. Girardeau-Montaut, J.Appl. Phys. **65**, 2889 (1989).
14. T. Anderson, I.V. Tomov and P. M. Rentzepis, J. Appl. Phys. **71**, 5161 (1992).
15. C. Girardeau-Montaut and J. P. Girardeau-Montaut, Appl. Phys. Lett. **55**, 2556 (1989).
16. N. A. Dyson, "X-ray in atomic and nuclear physics", Cambridge Univrsity Press, 1990.
17. C. E. Dick, A. C. Lucas, J. M. Motz, R. C. Placious, and J. H. Sparrow, J. Appl. Phys. **44**, 815 (1973).
18. M. Green and V. E. Cosslett, Proc. Phys. Soc. Lond. **78**, 1206 (1961).
19. I. V. Tomov, T. Anderson, and P. M. Rentzepis, Appl. Phys. Lett. **61**, 1157 (1992); **61**, 3193E (1992).
20. M. M. Murnane, H. C. Kapteyn, and R. W. Falcone, Appl. Phys. Lett., **56**, 1948 (1990).
21. Y. Kamamura, K. Toyoda and M. Kawai, Appl. Phys. Lett. **45**, 307 (1984).

22. S. W. Doweny, L. A. Builta, D. C. Moir, T. J. Ringler and J. D. Saunders, Appl. Phys. Lett. **49**, 911 (1986).
23. T. Q. Qui, C. L. Tien, Int. J. Heat Mass. Transfer 35, 719, (1992)
24. T. Q. Qiu and C. L. Tien, J. Heat Transfer, **115**, 842 (1993), and references therein.
25. T. Q. Qiu and C. L. Tien, J. Heat Transfer, **115**, 835 (1993).
26. S. D. Brorson, J. G. Fujimoto and E. P. Ippen, Phys. Rev. Lett., **59**, 1962 (1987).
27.. H. E. Elsayed-Ali and T. Juhaz, Phys. Rev. B, **47**, 13599 (1993).
28.. H. E. Elsayed-Ali and J. W. Herman, Appl. Phys. Lett., **57**, 1508 (1990).
29. H. C. Chen, G. A. Mourou and R. S. Knox, Mat. Res. Soc. Symp. Proc., **157**, 437 (1990).
30. B. C. Larson, C. W. White and T. S. Noggle, Phys. Rev. Lett., **48**, 337 (1982). B. C. Larson, J. Z. Tischler and D. M. Mills, J. Mater. Res., **1**, 144 (1986).
31. J. S. Wark, R. R. Whitlock, A. A. Hauer, J. E. Swain and P. J. Solone, Phys. Rev. B **40**, 5705 (1989).
32. B. VanWonterghem and P. M. Rentzepis, Proc. SPIE, **1204**, 784 (1990).
33. T. Anderson, I. V. Tomov and P. M. Rentzepis, J. Chem. Phys., **99**, 869 (1993).
34. I. V. Tomov, T. Anderson and P. M. Rentzepis, J. X-ray Sci. Technol., **4**, 44 (1993).
35. J. P. Girardeau-Montaut and C. Girardeau-Montaut, J.Appl. Phys. **65**, 2889 (1989).
36. C. Girardeau-Montaut, J. P. Girardeau-Montaut and H. Leboutet, Appl. Phys. Lett. **55**, 2556 (1989).
37. J. H. Bechtel, J. Appl. Phys., **46**, 1585 (1975).
38. N. Bloembergen, Mat. Res. Soc. Symp. Proc., **51**, 3 (1985).
39. R. W. James, "The Optical Principles of the Diffraction of X-rays", Ox Bow Press, Woodbridge, Connecticut, 1982.
40. V. F. Sears and S. A. Shelley, Acta Cryst., **A47**, 441 (1991).
41. American Institute of Physics Handbook, 3rd ed. (MaGraw-Hill, N.Y., 1972).
42. Y. S. Touloukian, R. W. Powell, C. Y. Ho and P. G. Klemens, eds. "Thermophysical properties of matter", IFI/Plenum, N.Y., 1970.

X. Figure Captions

Fig. 1. Schematic diagram of a planar x-ray photodiode.

Fig. 2. High repetition rate laser system for generation and amplification of picosecond pulses at 193 nm.

Fig. 3 a) Experimental set-up for x-ray output diagnostics and picosecond time-resolved x-ray diffraction. b) Schematic diagram of the X-ray CCD detector. c) Schematic representation of the X-ray streak Camenra

Fig. 4. a) Streak camera data showing UV and x-ray pulsewidths accumulated in videoprocessor memory. b) Scans of the UV and x-ray pulse images provide observed pulse duration of 51 ps and 128 ps, (FWHM) respectively.

Fig. 5. X-ray pinhole picture of the anode.

Fig. 6. X-ray energy as a function of the applied voltage.

Fig. 7. CCD image of the diffracted x-rays from Pt (111) crystal. X-ray diffraction signals from unheated and heated parts of the crystal are separated by a metal screen.

Fig. 8. Averaged pixel values of the diffracted x-rays from two consecutive 30 min. exposures. The signal strength is averaged over 20 pixels along the vertical axis and scanned along the horizontal axis of Fig 7. The first exposure is without UV heating: a) reference signal from unheated area and b) diffracted intensity from t he area where heating will take place. The second exposure when UV heating was applied: c) Reference.

Fig.9. CCD image of the diffracted x-rays from the Au (111) crystal. The CCD binning is x2 along the horizontal axis and x4 along the vertical axis. Note tilting of the image in the heated area.

Fig. 10. Time resolved x-ray diffraction data. Intensity ratio (I_{hot}/I_{cold}) vs. time.

Fig.11. Heat induced shift in the x-ray diffraction. Averaged pixel values of the diffracted x-rays from two consecutive 30 min. exposures. The signal

strength is averaged over 20 pixels along the vertical axis and scanned along the horizontal axis. Solid curve represent exposures with picosecond UV heating and the dashed curve correspond to x-ray diffraction without heating. a) - heated area, b) - unheated, reference, area.

XI. Tables

Table I. Quantum efficiency of electron photoemission from metals

l [nm]	193	211, [14]	248, [21]	263, [14]	266, [11]
Material		quantum efficiency (10^{-5})			
Aluminum	46.5	9.5	9.0	2.6	
Silver		28.4		2.6	2.0
Copper	6,[22]	28.6	2.0	0.84	14.7
Zinc		24.7	5.5	1.4	1.4
Nickel		17.7		0.88	2.5
Gold		16.2		1.1	4.7
Molybdenum		14.4		0.49	
Yttrium		13.9		1.4	50.0
Tantalum		12.5		0.94	1.0
Terbium		8.9		0.61	23.5
Samarium		6.8		0.47	72.5

Table II. Production of Ka photons from thick copper targets at different electron energies.

Electron energy [keV]	max charge/pulse [pC/mm^2]	efficiency [Ka photon/electron Sr]	Ka photons/pulse Sr
25	22.1	1.5×10^{-4}	2.07×10^{4}
50	44.3	5.2×10^{-4}	1.44×10^{5}
75	66.4	1.2×10^{-3}	4.97×10^{5}
150	132.8	2.8×10^{-3}	2.32×10^{6}
300	256.8	3.5×10^{-3}	5.80×10^{6}

75	66.4	1.2×10^{-3}	4.97×10^{5}
150	132.8	2.8×10^{-3}	2.32×10^{6}
300	256.8	3.5×10^{-3}	5.80×10^{6}

Table III. Relevant parameters of gold and mica.

Parameter	gold[18]	mica[19]
Reflectivity at 193 nm	0.21	
Radiation penetration [nm]	13.3	
Thermal conductivity - k [W/cm K]	3.15	0.0067
Specific heat - C_p [J/g K]	0.129	0.124
Density - r [g^{-3}]	18.88	2.85
Linear expansion coefficient [K^{-1}]	1.42×10^{-5}	

XII. Pertinent Papers and Patents

1. Ultrashort Time-Resolved X-ray Source. Lasers Int. P. M. Rentzepis 89, 16, 1989
2. Performance of Metal Photocathodes in a Picosecond Pulsed Laser Driven X-ray Diode, B. Van Wonterghem and P.M. Rentzepis, *Appl. Phys. Lett.*, 56, 1005 1990.
3. Application of a novel picosecond pulsed laser driven x-ray source in time resolved diffraction experiments. B. Van Wonterghem, P.M. Rentzepis Proc. Int. Conf. on Lasers Soc. of Optics and Quantum Electronics 27, 788 (1990).
4. Generation of picosecond x-ray pulses and their application in picosecond time resolved x-ray diffraction B. Van Wonterghem, P.M. Rentzepis Proceedings SPIE. Vol 1204 ,784 (1990)
5. Picosecond X-Ray Difraction. B.Van Wonterghem and P.M.Rentzepis Soc.of Optical and Quantum Electronics, Proc. Int. Conf. on laser 28, 718, 1991.
6. Theoretical Study of Laser Heating and Dissociation Reactions in Solids Using Ultrasfast X-Ray Diffraction. H. Ma, S.H.Lin, P.M.Rentzepis J. Appl. Phys. 72,(6), 2174-2178, 1992
7. Some Applications of Ultrafast :Laser and Picosecond X-Ray Pulses. V. Sandh , P. M. Rentzepis. Trends in Chemical Physics 2, 129- 143 1992
8. Laser Driven Metal Photocathodes for Picosecond Electron and X-Ray Pulse generation. Todd Anderson, I. V. Tomov, P. M. Rentzepis JAP, 71, 5161-5167, 1992.
9. High repetition rate picosecond laser system at 193 nm. I.V. Tomov. T . Anderson and P. M. Rentzepis Appl. Phys. Lett. 61, No 10, 1157-1159. 1992.
10. A high Repetition rate Picosecond Hard X-Ray System and its Application to time resolved X-ray Diffraction. T . Anderson, I.V. Tomov and P. M. Rentzepis. J. Chem Phys. 99, (2), 869-875, 1993
11. Picosecond X-Ray pulses Generated in a Diode Driven By 193 nm Picosecond Laser Pulses. I.V. Tomov, T Anderson, P. M. Rentzepis J. X-Ray. Sci. and Tech. 4, 44-56, 1993

12. Efficient Raman Conversion of High Repetition Rate, 193 nm Picosecond Laser Pulses. I. Tomov, Peilin Chan and P. M. Rentzepis. J. Appl. Phys. (Submitted 2/2/94)
13. Picosecond time resolved x-ray diffraction during laser pulse heating of Au (111) crystal I. V. Tomovc, P. Chen ,P.M. Rentzepis, Appl. Phys. Lett.(Submitted 4/15/94)
14. Patent. Ultrashort time resolved X-Ray Source P.M. Rentzepis. Patent Number 5,042,058 date of issue August 20, 1991
15. Compact High-intensity pulsed x-ray source, particularly for lithography. Patent applied for (filed August 20, 1991) Peter M. Rentzepis.

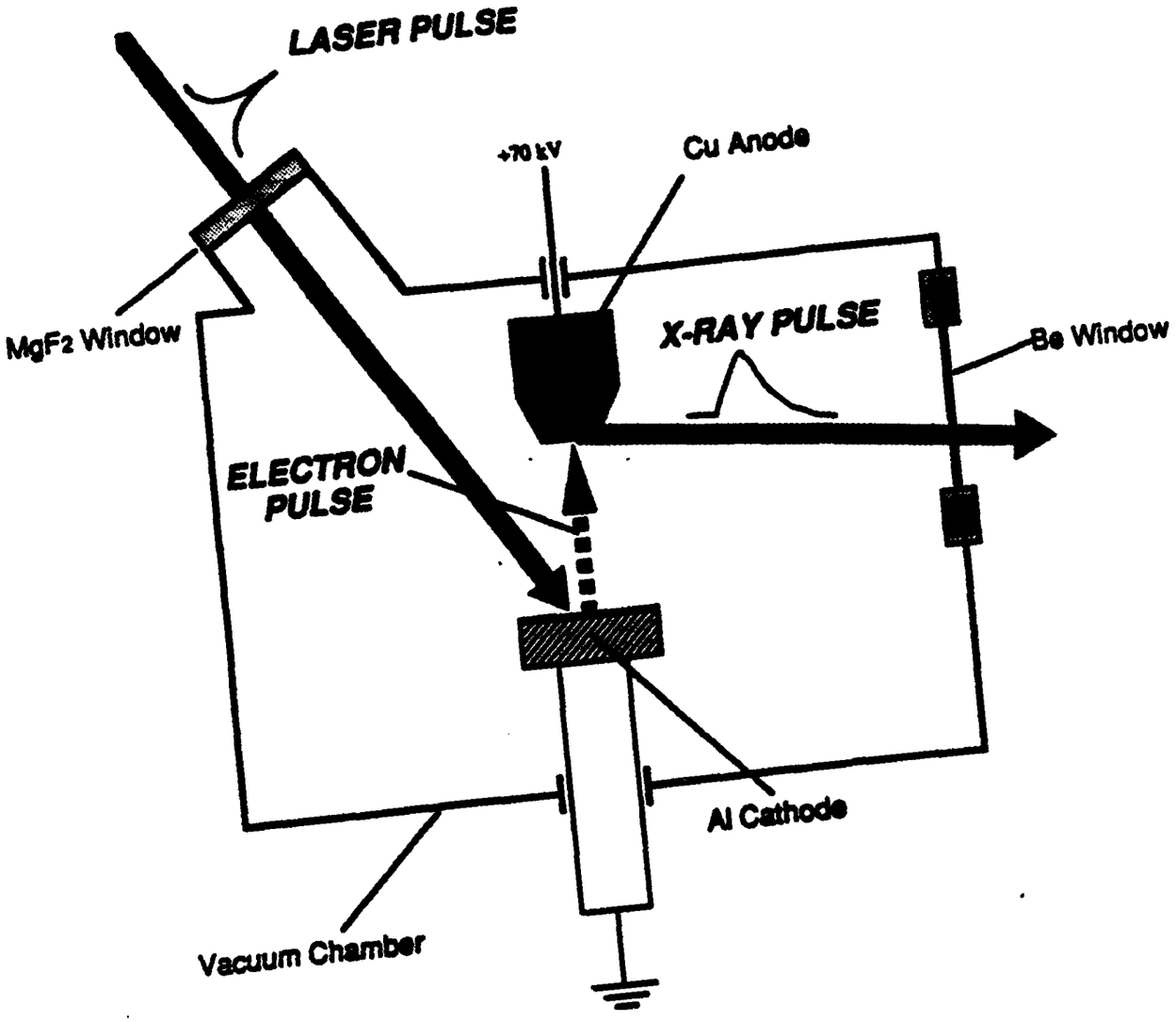
LASER PULSE
+70 kV
Cu Anode
MgF2 Window
X-RAY PULSE
Be Window
ELECTRON PULSE
Al Cathode
Vacuum Chamber

Figure 1

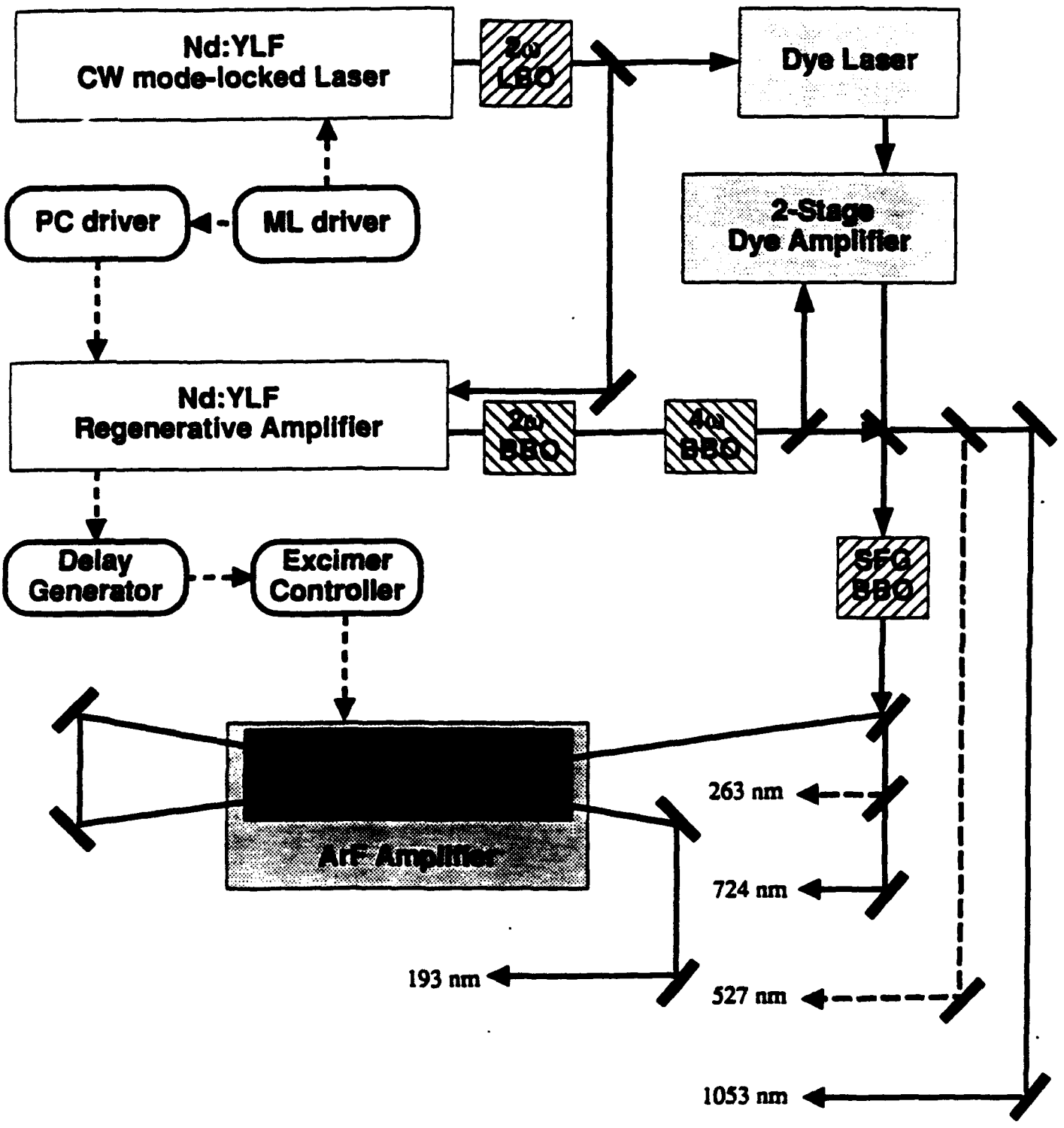
Nd:YLF
CW mode-locked Laser
2ω
LBO
Dye Laser
PC driver
ML driver
2-Stage
Dye Amplifier
Nd:YLF
Regenerative Amplifier
2ω
BBO
4ω
BBO
Delay
Generator
Excimer
Controller
SFG
BBO
ArF Amplifier
263 nm
724 nm
193 nm
527 nm
1053 nm

Figure 2a

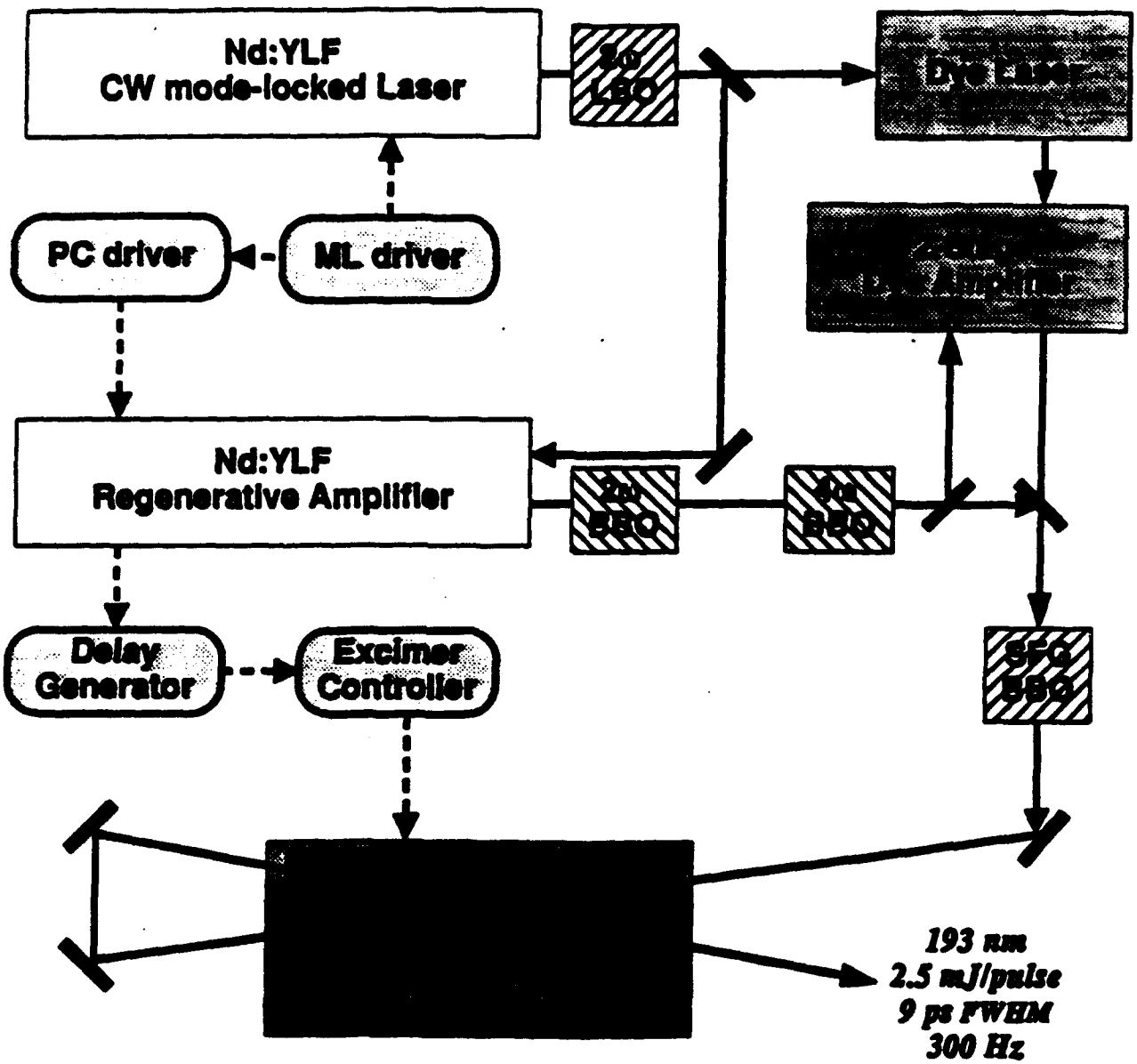
Nd:YLF
CW mode-locked Laser
PC driver
ML driver
Nd:YLF
Regenerative Amplifier
Delay
Generator
Excimer
Controller
193 nm
2.5 mJ/pulse
9 ps FWHM
300 Hz

Figure 2b

SAMPLE AND DETECTOR CONFIGURATION

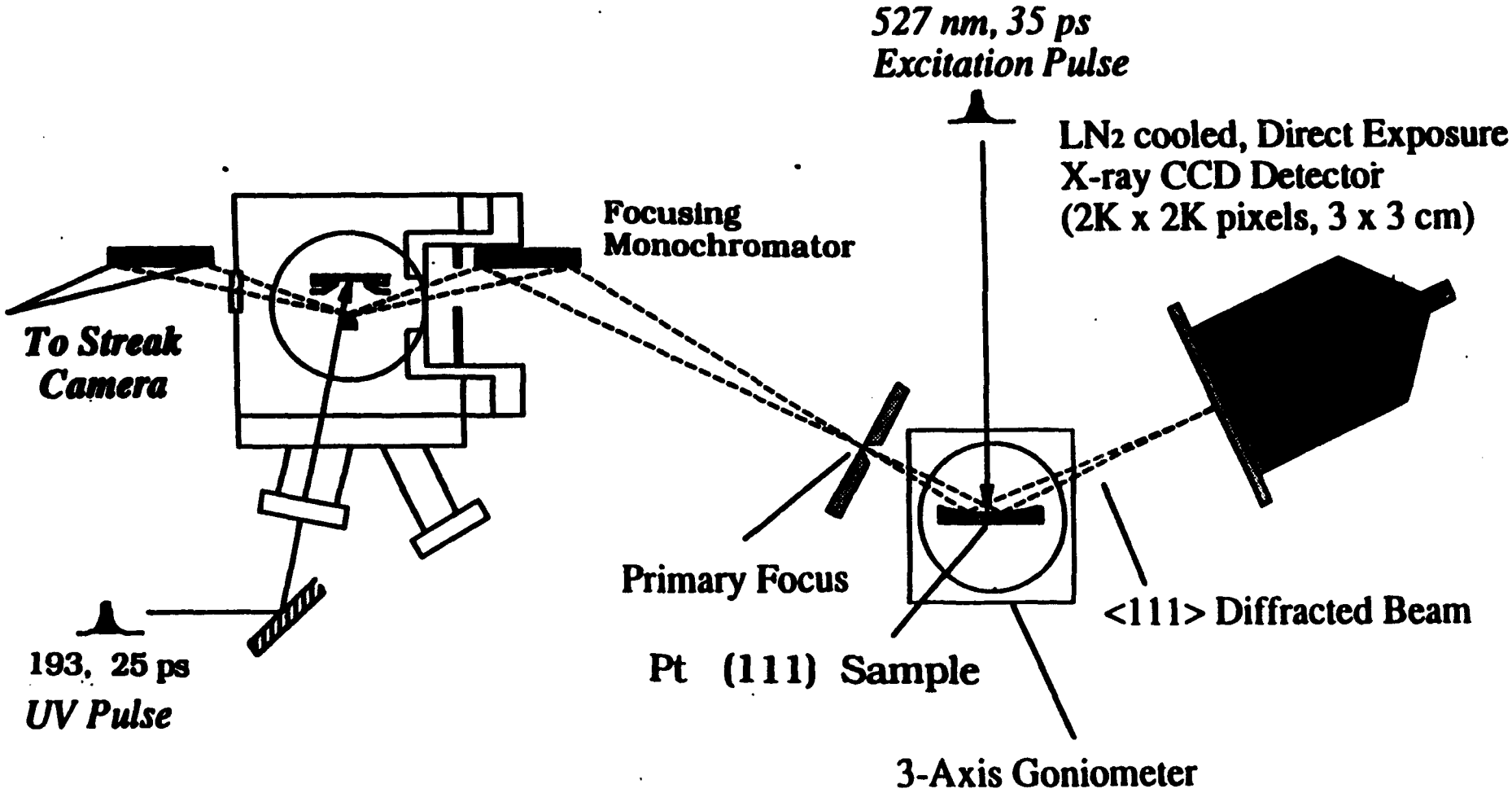

Figure 3a

DIRECT X-RAY IMAGING DETECTOR USING LARGE AREA CCD

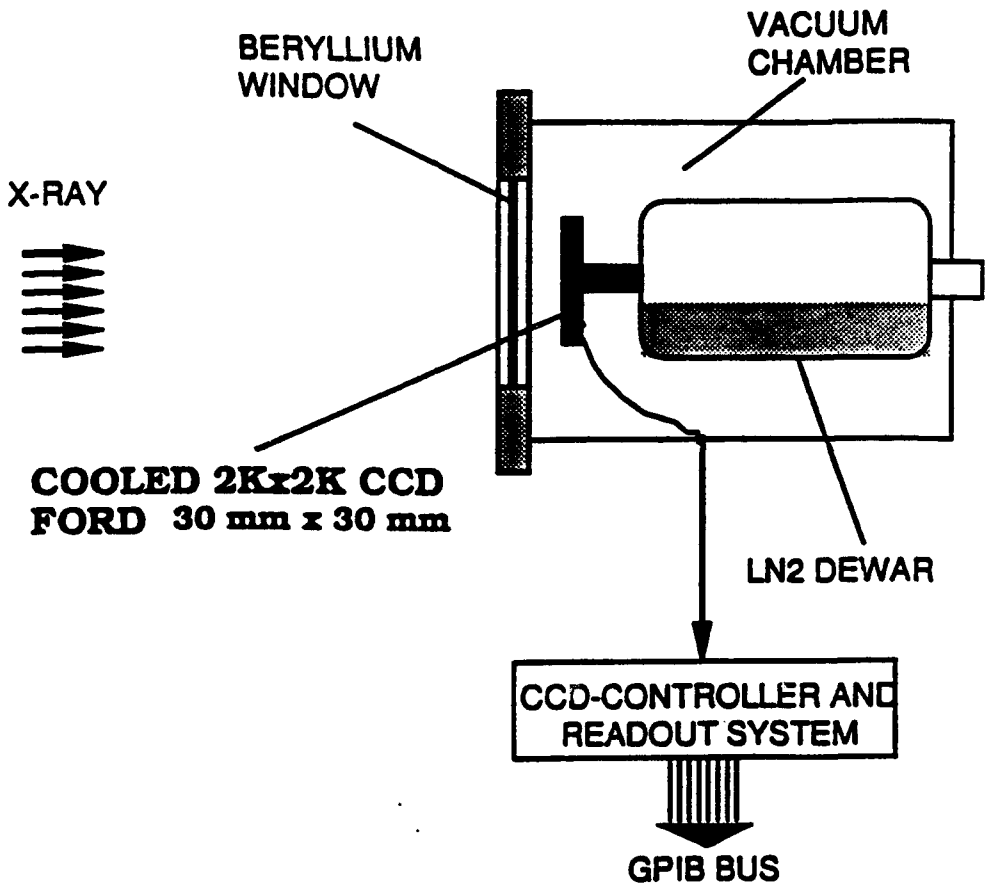

Figure 3b

X-RAY POSITION SENSITIVE DETECTORS

PHOSPHOR-SCREEN BASED X-RAY DETECTOR
PHOSPHOR + IMAGE INTENSIFIER + CAMERA

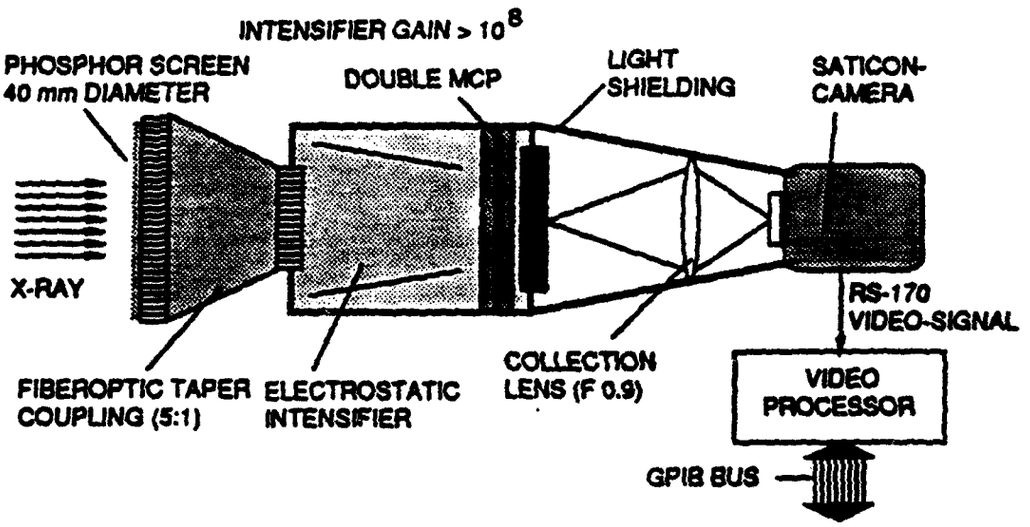

Figure 3c

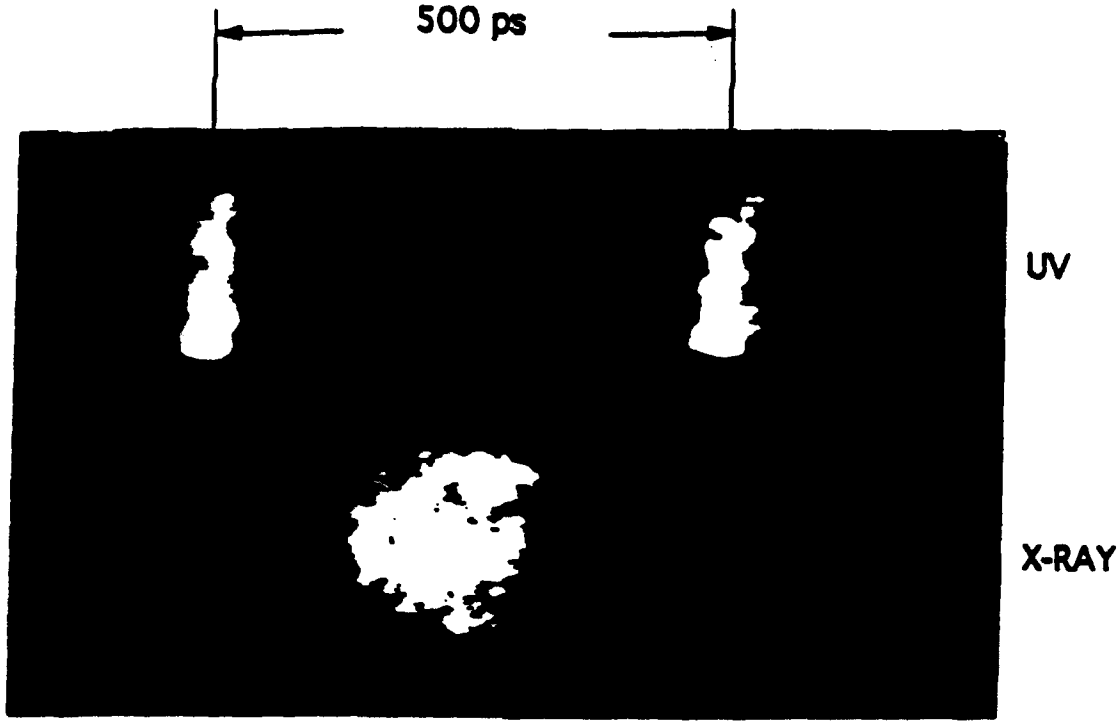

Figure 4a

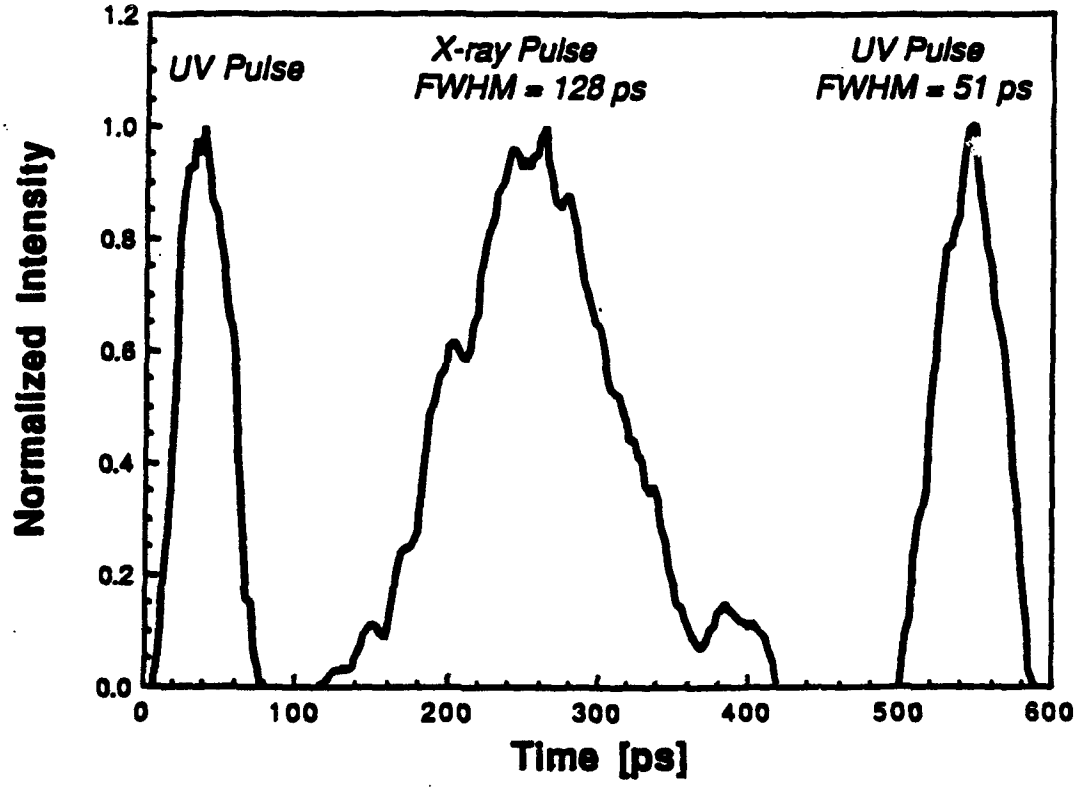

Figure 4b

Figure 5

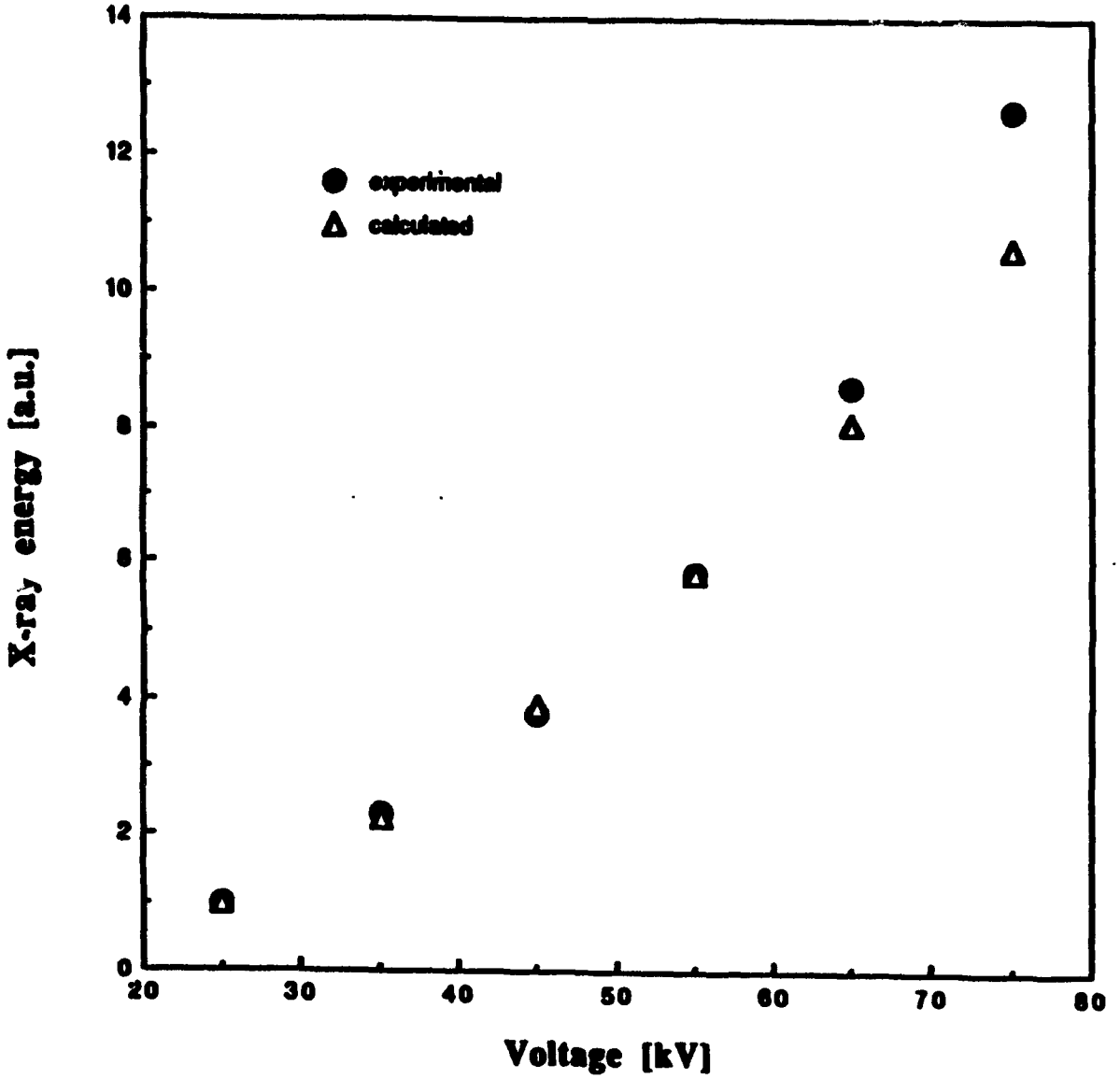
experimental
calculated
X-ray energy [a.u.]
Voltage [kV]
0
2
4
6
8
10
12
14
20
30
40
50
60
70
80

Figure 6

Figure 7

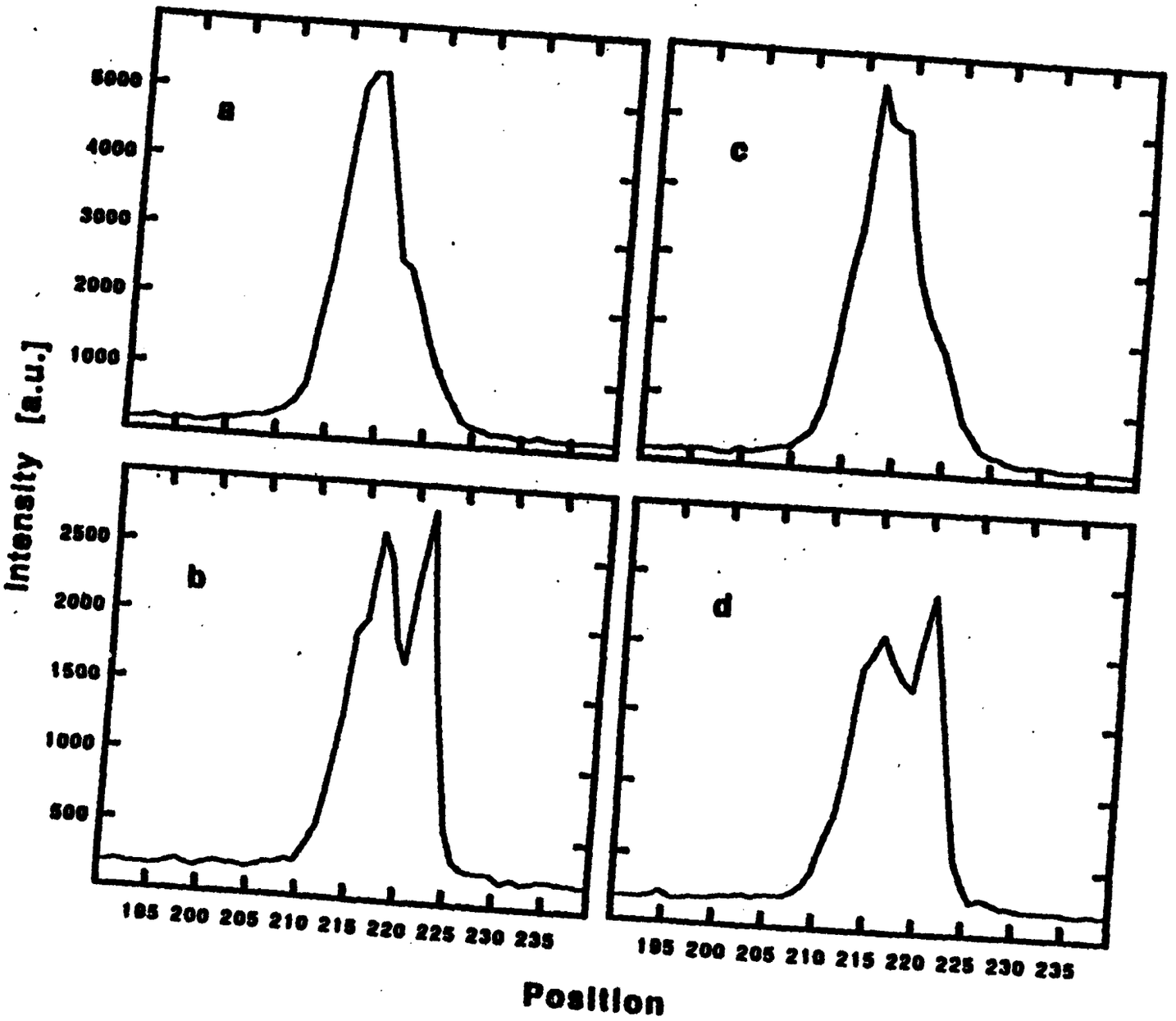
a
b
c
d
Intensity [a.u.]
5000
4000
3000
2000
1000
2500
2000
1500
1000
500
185 200 205 210 215 220 225 230 235
185 200 205 210 215 220 225 230 235
Position

Figure 8

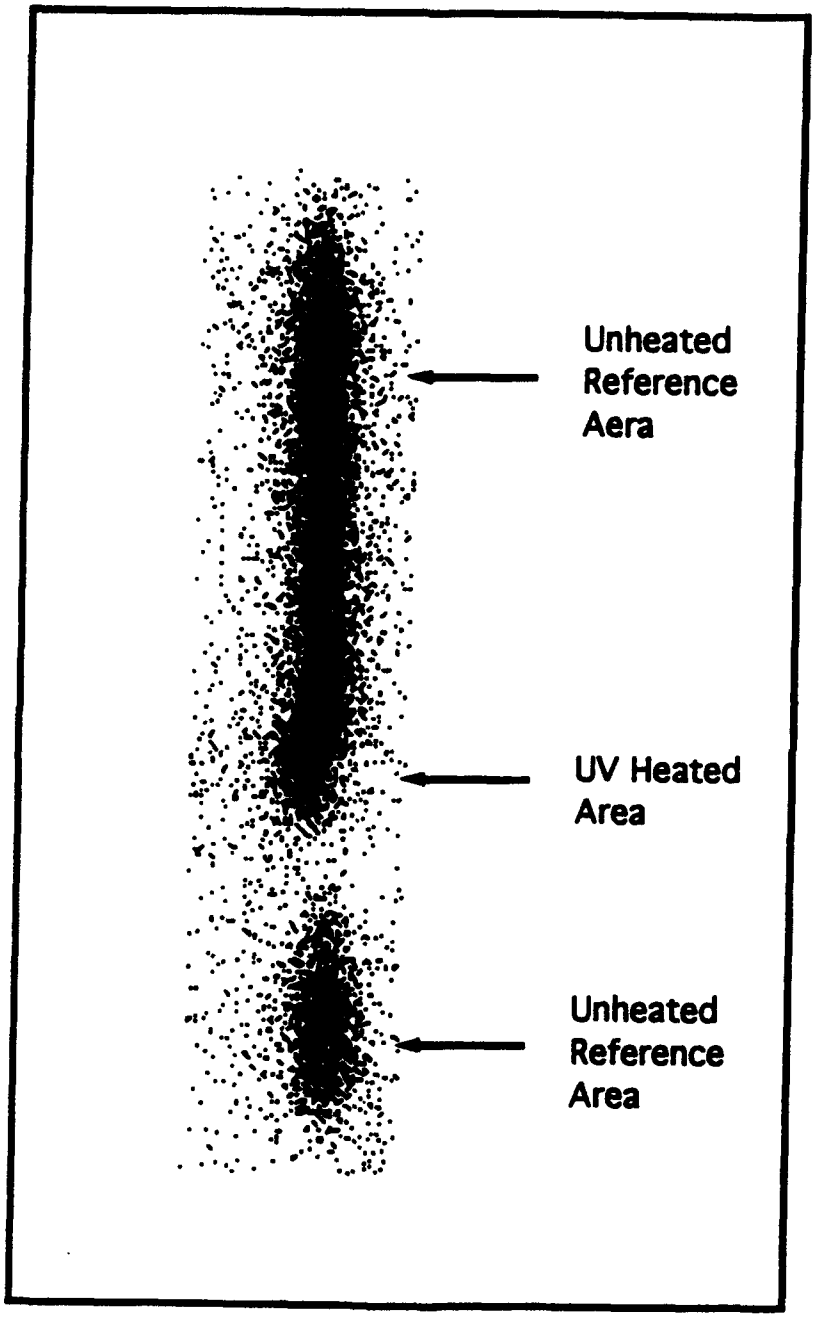
Unheated
Reference
Aera
UV Heated
Area
Unheated
Reference
Area

Figure 9

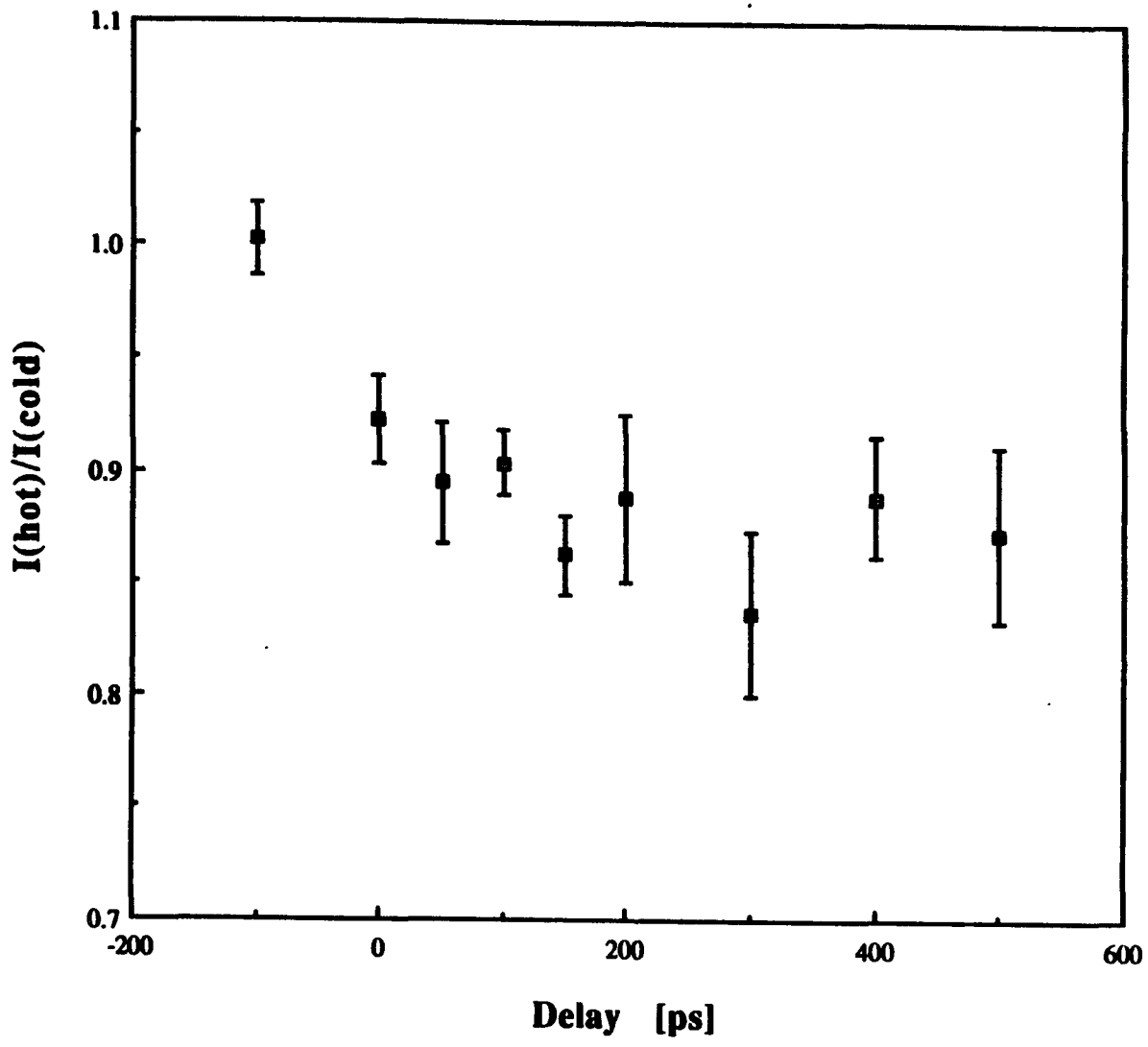

Figure 10

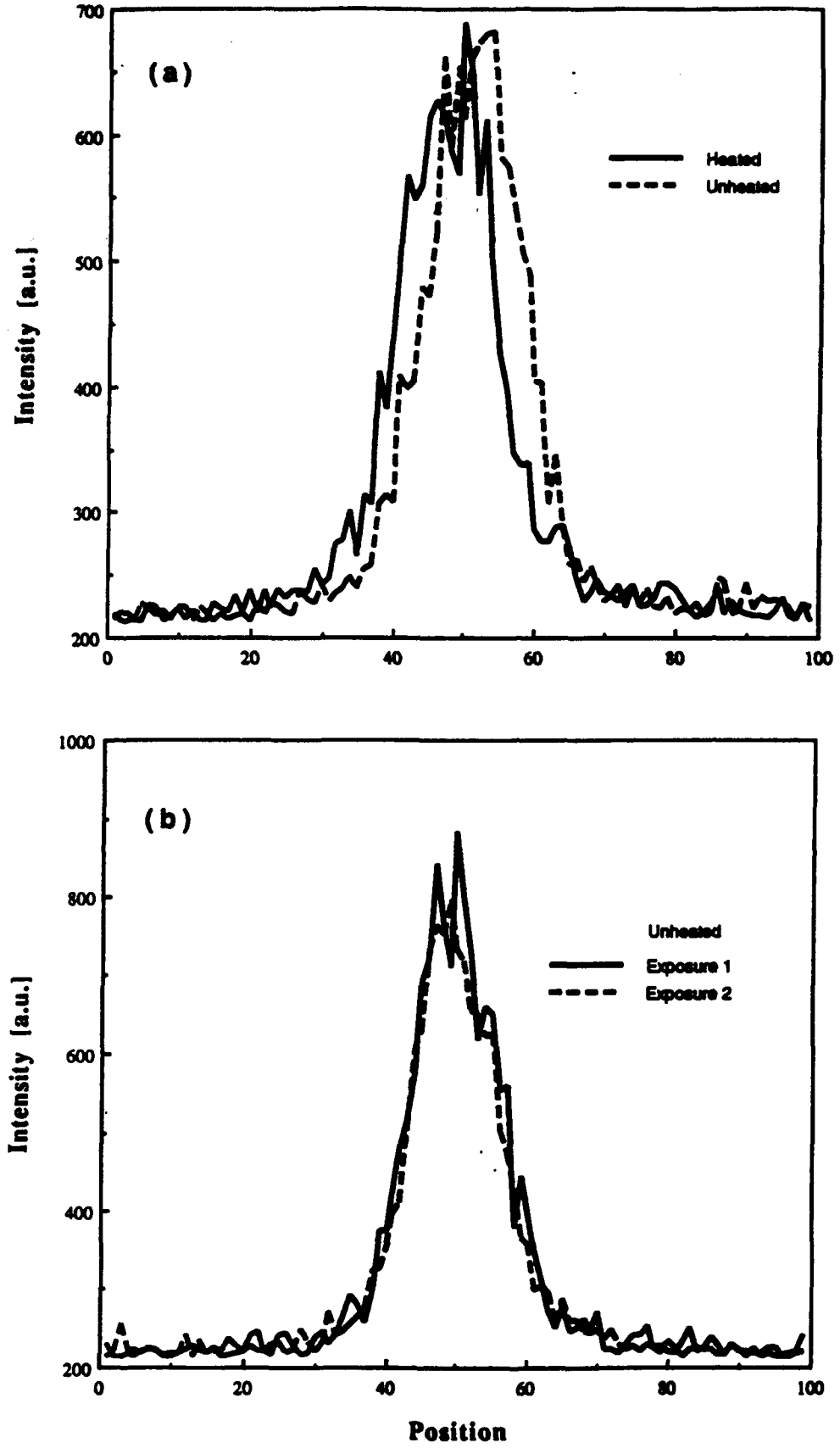
(a)
Heated
Unheated
Intensity [a.u.]
700
600
500
400
300
200
0
20
40
60
80
100
(b)
Unheated
Exposure 1
Exposure 2
Intensity [a.u.]
1000
800
600
400
200
0
20
40
60
80
100
Position

Figure 11